

# Environmental Sensing using Hyperspectral Imaging

Bhavyashree S<sup>1</sup>, Ruhin Kouser R<sup>2</sup>

*Computer Science and Engineering  
Presidency University*

\*\*\*

**Abstract** - HSI is an emerging technology for environmental sensing that provides high-resolution spectral data across many applications. It is key to monitoring air quality, water resources, soil properties, and vegetation health. It is essential for addressing global challenges like climate change, pollution, and sustainable resource management. The ability to collect and analyze data across many spectral bands gives unparalleled insights, allowing for precise detection and monitoring of environmental changes. Despite this, HSI faces many challenges such as high cost, limited datasets and calibration complexities preventing accurate analysis requires advanced computational resources. This review article will discuss the challenges and future advancements that are necessary for environmental sensing. HSI technical advancements have focused on increasing spatial resolution, portability, and low cost. Innovations like drone-mounted hyperspectral sensors, machine learning models for data analysis, and cloud computing have made the technology more accessible and applicable. This allows for real-time environmental monitoring, enabling prediction and providing better responses to environmental issues. Using advanced technologies it can overcome all these limitations of HSI. Distributed processing and edge computing can handle big data more efficiently, low-cost sensors and advanced algorithms are being developed to make it cost-effective and accurate. By enabling real-time environmental monitoring and informed decision-making, HSI will help for a sustainable future and its continued evolution will empower researchers and policymakers to address environmental issues more efficiently.

**Key Words:** optics, photonics, light, lasers, templates, journals

## 1. Introduction

The UN Sustainable Development Goals (SDGs) enable a framework for sustainable development, ensuring a better world by balancing social, economic, and environmental dimensions while addressing broader challenges such as health, and climate [1-3]. Recent progress considers plant phenotypic plasticity and responses to climate change through environmental sensing and signaling [4]. The SDG targets for water and sanitation require detailed monitoring and response to understand the coverage and quality of safely managed sources [5]. Therefore, real-time monitoring is essential for addressing climate change and improving water and sanitation,

tracking pollutants, and ensuring compliance with sustainability goals. Environmental sensing is crucial in monitoring air, ecological health, and water by identifying the challenges related to industrialization by providing high-quality, high-resolution images [6] and urbanization by improving city environments and avoiding resource waste [7] and biodiversity loss by tracking data and easily available to policymakers [8].

Monitoring air quality is essential because particulate matter (PM<sub>2.5</sub>) and PM<sub>10</sub> which are fine particles affect the eyes, nose, and throat and can make the lungs dysfunctional [9, 10]. Therefore, knowing the concentration of air pollution is crucial to protect human health. Van Donkelaar, A., et al., developed a technique for estimating PM<sub>2.5</sub> exposure by combining satellite and ground-based data into the Data Integration Model for Air Quality (DIMAQ) [11, 12]. A Beta Attenuation Monitor (BAM) uses the principle of ray attenuation to measure the mass concentration of PM in ambient air [13]. It has high measurement accuracy, easy maintenance, and low cost but low temporal resolution and loss of volatile substances in PM. The tapered element oscillating microbalance (TEOM) with high accuracy, high sensitivity, and high temporal resolution [14] overcomes the disadvantage as it measures PM concentrations using a hollow oscillating microbalance to detect and report changes in mass as ambient air passes through a replaceable filter [15, 16]. Kinsey, J.S., et al., demonstrated a method that compares BAM with TOEM PM mass concentration, where TOEM was the best overall correlation [17]. The drawback of the TEOM instrument is the requirement to maintain the filter at a constant temperature, which can vary based on location, environmental conditions, and concentration levels [18].

Water pollutants severely threaten human health and aquatic ecosystems [19]. It mainly consists of nitrogen, phosphorous, chlorophyll, heavy metals, biological oxygen demand (BOD), and chemical oxygen demand (COD) [20]. Increased BOD and COD concentrations can cause the death of aquatic animals, and plants [21]. Water quality monitoring is more efficient for preventing pollution [22]. Using a multi-wavelength optical sensor, the light-emitting diodes (LED) sources can be measured and transmitted through water and absorb light at specific wavelengths, it is a robust, easily deployable sensor [23, 24]. Attivissimo, F., et al., proposed a cheap optical sensor for the detection of low chlorophyll levels (such as 0.5 – 8.0 µg/l) in marine water and higher concentration levels (about 200

$\mu\text{g/l}$ ) in seawater and based on chlorophyll fluorescence [25]. Excess phosphorus and nitrogen concentration increase algae's abnormal growth, resulting in eutrophication [26, 27]. Studies by Li, Z., et al. have shown that remote sensing of Ch, N, and P vegetation biochemical properties is conducted using narrow-band spectral indices from ground and space hyperspectral data [28]. Jupp, D.L., et al., have shown that detecting algae in surface layers of turbid waters can be based on chlorophyll-a (Chl-a) absorption using airborne scanning [29]. Chang, N.-B., et al., used space-borne satellite images, and airborne remote sensing nutrients to improve water quality [30]. Gholizadeh., et al., combined various properties such as spectral, spatial, and temporal using optical sensors with spaceborne and airborne sensors to be used as a sensor selection [31]. The disadvantages of optical sensors are that they are high-cost, the system requires skilled operators, and more sensitive detectors [32]. They can be overcome by combining HSI with a machine learning (ML) algorithm to enhance the understanding of pollutants by providing real-time data, and detailed information [33].

Hyperspectral sensors capture the image in hundreds of spectral bands including visible wavelength (380nm–700nm), near-infrared (800–2500 nm), and mid-infrared (2500–15000 nm) [34, 35]. Different spectral bands are present in each pixel to extract particular information about various pollutants [36]. HSI captures the data cube to contain 1D spectral and 2D spatial information [37, 38]. A 1D spectrum represents how the pollutants at a pixel absorb light across different wavelengths, and 2D vectors represent each pixel location in the spectrum in a spatial array [39]. HSI has been utilized in various remote sensing applications to estimate the physical characteristics of complex surfaces and detect similar pollutants with fine spectral signatures [40]. The traditional RGB method uses only three primary colors [41] by combining different light intensities. At the same time, multispectral imaging (MSI) is built on RGB that captures (3-10) spectral bands that are non-contiguous in the electromagnetic spectrum [42]. HSI is superior to any other broadband image, as it can provide more detailed information. HSI is used in plant detection [43], chemical imaging [44], medical analysis [45], and mining [46].

Therefore, integrating environmental sensing with HSI technology proposes low-cost, accurate data on air and water detection and protects ecosystem health.

## 2. Fundamentals of Hyperspectral Imaging

In HSI applications, illumination units such as tungsten and halogen lamps, LED, lasers, and tunable lights are utilized for light-source management across wavelengths [47]. Electric and magnetic fields combine to form an electromagnetic wave referred to as light [48], that can be refracted, absorbed, or reflected on the surface [49] with different materials responding to specific wavelengths. For instance, the primary light reflected by a yellow rubber duck is from the middle, and longer wavelengths are absorbed by shorter wavelengths which

do not reach the observer [50]. When radiation is captured across multiple wavelengths on a wide spectral band, identifying and categorizing materials is possible using the resulting spectral signature by unique spectral properties [51, 52]. This data is structured into a data cube a set of coregistered 2D images for each wavelength band [53]. To improve the interpretability of datasets, Principal Component Analysis (PCA) can be employed to reduce their dimensionality and minimize information loss [54, 55]. Reduced-dimensionality features are fed into artificial neural networks and ML algorithms for classification [56]. Optical equipment comprised a scanning microscope and imaging spectrographs that utilized silicon and InGaAs CCD diode array detectors, enabling direct comparison between the intensity of near-infrared reflectance (NIR) and exNIR light transmitted through different samples [57, 58].

### 2.1 Spectral Imaging Methods

In remote sensing, HSI is captured using pushbroom or whiskbroom scanning methods, which involve line-based scanning and exploit the motion of an airborne platform to collect images [59]. Whiskbroom (also known as a point scanner) has a rotating mirror that scans the surface point by point to build a 2D image by capturing light from each pixel across the flight path, passing it through the dispersion element, measuring it with a 1D detector array, with different wavelengths recorded by separate array elements [60, 61]. Its advantages include a simple design, wide swath coverage, and easy calibration. Qian, S.-E., explains that the Airborne Visible/Infrared Imaging Spectrometer (AVIRIS), the first operational airborne hyperspectral imager, was developed in the mid-1980s and the Compact Airborne Spectrographic Imager (CASI), the first commercial airborne hyperspectral instrument, was produced in the late 1980s [62]. Reuter, D.C., et al., outline that Landsat instruments used during the spacecraft traveled in the along-track direction, and moving mirroring was utilized to sweep detectors for each channel [63]. Kampe, T.U., et al. demonstrated the NEON spectrometer's performance requirements have been well-established through the development of the NASA AVIRIS program and the Carnegie Airborne Observatory [64]. However, whiskbroom has drawbacks, such as high spatial and spectral resolution constraints because of low integration times, which require a mechanical scanner with moving parts in a vacuum chamber [62]. Funatomi, T., et al., used a method to terminate the temporal illumination variations in whiskbroom HSI by adding a pushbroom scan [65]. To overcome these limitations, the pushbroom sensor was developed [66], and each spatial element has its detector, where integration times are much longer and no requirement of moving parts can achieve the same signal-to-noise ratio (SNR) as a whiskbroom with slight entrance pupil [63]. Tarde, R.W., et al., demonstrated the use of pushbroom technology which eliminates the need for large calibration shutters and diffusers, resulting in better signal-to-noise performance with smaller optics, an ideal solution to data

acquisition. This improves reliability and performance, by developing small and low-cost instruments [67].

In a pushbroom, the dataset is acquired by scanning the sample line by line to form the hypercube [68]. Each line image constitutes a single band of the hyperspectral data, with a 1D detector array representing spectral and spatial information [47, 69]. A pushbroom camera has an optical system that projects an image onto a linear array of sensors, imaging only the points in the plane defined by the optical center and the line containing the sensor array [70]. In pushbroom, the platform's movement allows the sensor to project a continuous, linear scan of the ground surface onto the camera focal plane as it travels along its path [71]. Johnson, B.R., et al., overviews a CASI developed for airborne remote sensing using pushbroom imaging spectrometers [72]. Gartley, M. and J. Schott., gathered information about the Advanced Land Imager (ALI) and the impending Landsat 8 Operational Land Imager (OLI) payload is designed to operate in a pushbroom which is common to commercial high-resolution [73]. Tarde, R.W., et al., explained the development of the next-generation OLI pushbroom filter radiometer, capable of meeting challenging radiometric and calibration requirements [67]. A sensor model incorporating radiometry and orbital mechanics has shown a field-of-view (WFOV) [74]. The emitter is difficult for multisubstrate filters with soft coatings, as these filters require parallelism within a few arc seconds [75].

The staring (also known as the band sequential method) is a spectral scanning technique that essentially produces a 2-D grayscale image with all spatial information at once [76]. To obtain high-resolution images, staring array imaging satellites usually adopt the low Earth orbit and gradually develop toward submeter high-resolution and night-light imaging [77]. Magnan, P., explained the key features of CCD, such as a minimum read noise, low dark current, and a high level of quantum efficiency [78]. Bhan, R. and V. Dhar., explain the signal photon detection, optical wave band selection (BS) and transmission, and multiplexing of parallel and serial out signals are undertaken by FPA's hybrid architecture [79]. Gupta, N. developed MEMS-based FP filters to minimize the dimensions of staring hyperspectral imagers [80]. The staring array has limited spectral resolution due to a low number of spectral filters, is not suitable for research [81], and sampling limitations cause aliased signal that corrupts the image by pre-sample blur, post-blur, or sampling frequency [82]. The use of new scanning technology, particularly staring focal plane array (FPA) introduces new parameters influencing system performance that are not adequately addressed by existing models [83]. Li, P., et al., designed a real-time attitude controller for staring, and the output is based on the prediction of the future [84].

Snapshot (also known as single-shot) acquire 2D spatial and 1D spectral information in a single shot [85], offering low memory requirements, fast acquisition speed, and potentially lower cost and power consumption [86], the efficiency of light collection is improved in high-dimensional measurement systems by

eliminating filtering and scanning [87]. Wagadarikar, A.A., et al., developed a mathematical model to describe SD-CASSI, how light is transmitted through the coded aperture, and how it affects the resulting data cube, outlining how the coded aperture modulates spatially each spectral slice of the data [88]. Snapshot hyperspectral cameras used for drones further increase the spectral resolution of data, often capturing hundreds of bands in a contiguous fashion from visible to NIR to short wave infrared (SWIR) ranges [89] they are used in applications that require vital observations such as industrial inspection, environmental monitoring, and medical diagnostics [90]. Among whiskbroom, pushbroom, and snapshot, the lightweight snapshot and pushbroom imagers have met the payload requirements of lightweight unmanned aerial vehicles (UAVs) in recent years. Snapshot images can capture an entire data cube in a single snapshot without scanning. Alternatively, a pushbroom imager acquires scanned data cubes while edging a moving platform and captures vertical slices simultaneously [91]. However, challenges faced in snapshot performance involve many computational loads, hardware complexity, trade-off resolution, and capture speed [90].

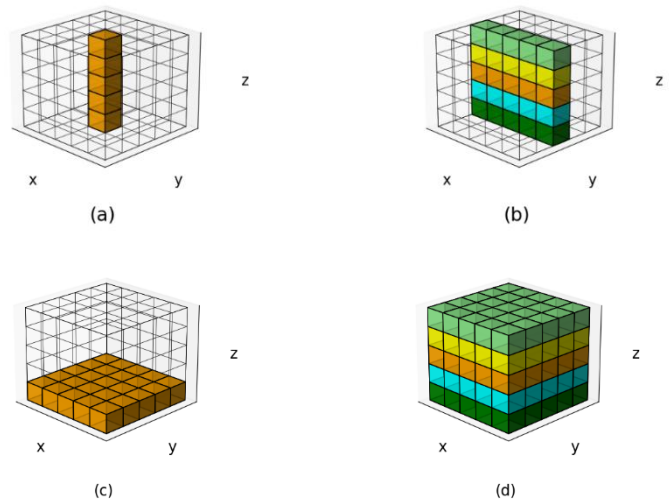


**Fig. 1** Spectral imaging approaches (a) Whiskbroom (b) Pushbroom (c) Staring (d) Snapshot

### 3. Applications of HSI in Air Quality Monitoring

HSI is essential for monitoring air pollution by identifying and measuring specific gases in the atmosphere. Hyperspectral sensors can detect reflectance and absorption variations. These sensors can be deployed on satellites, drones, or ground-based platforms to gather data across extensive areas. The high-resolution spectral data allows us to evaluate air quality, track pollution, and analyze pollutants. Furthermore, HSI can be integrated with machine learning to enhance the precision of monitoring pollution and policy development. A bottom-up spectroscopy technique to verify airborne HSI was introduced by Soffer, R.J., et al., which is compared with the calibration and validation (cal/val) targets focused on CASI imagery that

exhibits an improvement in the accuracy of reflectance product by optimizing the pixel location and applying the Spectral Band Ratio (SBR) process and the airborne hyperspectral reflectance (HCRF) data were relatively accurate for wavelength greater than 450 nm, with less than 4% error [92]. Xing, C., et al., developed an HSI to monitor aldehyde volatile organic compounds (VOCs), through ultraviolet light signals in the 300–380 nm spectral range and 0.6 nm resolution and extension of the 300–560 nm range, fitting of VOC releases was found by the differences in the range from 4 % to 19 % and the WRF-ARW 4.2 model introducing vertical hybrid pressure-sigma layers which are used for the transport [93]. Addabbo, P., et al., demonstrated a various method in improving atmospheric retrievals of trace gases, such as Weighting Function DOAS (WFDOAS), Blind Source Separation (BSS), and PCA, absolute errors in the calculated gas concentration ranging from  $10^{-2}$  to  $10^{15}$  mol/cm<sup>2</sup>, the spectral range of the Scanner Imaging Absorption Spectrometer for Atmospheric CHartography (SCIAMACHY) measures 383–628 nm spectral range and 0.44 nm of resolution, minimum error in retrieving the traced gases is limited to the (437.12–451.40) nm, nonpolluted environments ( $0 - 5 \cdot 10^{15}$  mol/cm<sup>2</sup>) and highly polluted environments ( $30 \cdot 10^{15}$  mol/cm<sup>2</sup>) [94]. An edge-based AI UAV system (ETAUS) was proposed by Huang, C.-H., et al., that combines HSI (380–780) nm with convolutional neural networks (CNN), the dataset in training, validation, and testing is 80%, 10%, 10% achieved an accuracy with 86.38% in terms of Air Quality Index (AQI) level classification, with 9.3 frames per second (FPS) real-time performance and speedup of 2.28× to 36.9× in FPS [95]. A quantitative assessment of different air pollution (QADAP) models at 500 m resolution was developed by Ahmadian Marj, A., et al., 54 satellite images with spectral and spatial resolutions consisting of 3 GeoEye, 1 Hyperion, and 50 MODIS images, lower relative Root Mean Square Errors (RMSE) were achieved from 13–25% at high pollution levels and 150–400% at low pollution levels, Correlation coefficients (R) ranging from 0.75 to 0.85 with good agreement [96]. To estimate PM<sub>2.5</sub> concentrations utilizing the multi-angle implementation of atmospheric correction (MAIAC) aerosol optical depth (AOD) satellite data was developed by Just, A.C., et al., a hybrid model with a mean cross-validated R<sup>2</sup> of 0.724, the predictions were slightly biased with cross-validated slopes of  $1.00 \pm 0.008$  and  $1.12 \pm 0.009$  of standard errors therefore, mean-predicted PM<sub>2.5</sub> concentrations were 19.7 to 27.2 µg/m<sup>3</sup> range [97]. An AI-powered learning-based low-cost air quality monitoring model was proposed by Su, X., et al., captured HSI with a resolution of  $512 \times 512 \times 204$  across 51 selected channels (400–1000) nm that was tested on 1,487 data points, with a Mean Absolute Error (MAE) of 698.65 meters and a coefficient of determination (R<sup>2</sup>) of 0.95 in EnvNet [98]. Kalajdjieski, J., et al., developed a CNN, ResNet, Inception, and a custom pre-trained Inception model for air pollution prediction that can classify the input images, a Generative Adversarial Network (GAN) enhanced with data augmentation techniques is used to handle the problem of imbalanced datasets

which leads to the improved performance, this model was tested on a dataset of 178792 images, and the results obtained indicate an accuracy of 89.6% and 76.3% in training and testing set [99]. Bakirci, M., et al., demonstrates a method for the vertical distribution and transport of pollutants combined with hexacopter UAV and miniature monitors through a commercial drone and with Real-Time Kinematic (RTK) capabilities, ensuring a level of accuracy of the measurement is high, using reliable sensors such as NOVA SDS011 and MICS-4514, resulting the zigzag drone flight patterns offering the good accuracy for pollution detection [100]. A deep learning method for predicting the AQI was developed by Janarthanan, R., et al., combining a Support Vector Regression (SVR) model and Long Short-Term Memory (LSTM) networks, the average RMSE is 7.804 for training and 10.995 for testing and R<sup>2</sup> for PM<sub>2.5</sub> is 0.821, resulting the best-performing pollutant [101]. A system for the spatio-temporal prediction of climate and environmental variables was introduced by Amato, F., et al., using CNN for spatial analysis and recurrent networks (RNNs) for temporal modeling, accomplishing the spatio-temporal signal that can be decomposed utilizing Empirical Orthogonal Functions (EOFs) with 95% of variance in the 24 components, achieving a MAE of 1.978 for deep learning, 6.709 for Random Forest (RF), and 8.34 for neural networks (NN) in the simulated datasets [102]. Din, A.U., et al., introduced a method to examine transport sustainability through spatial transportation efficiency relating to climate change, by Structural Equation Modeling (SEM) and AMOS with 410 respondent samples and simulation sampling of 10,000, with R<sup>2</sup> of 16% providing robustness to the model, RMSEA is 0.081, standardized root mean square (SRMR) is 0.060, and Goodness-of-Fit Index (GFI) is 0.949 measuring a good fitness [103].

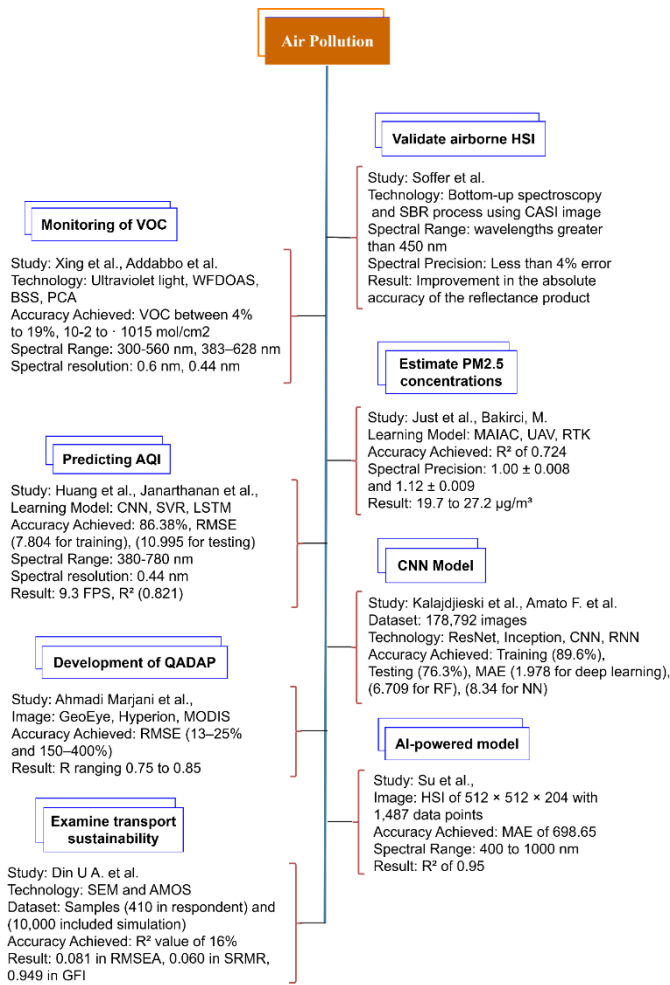


Fig. 2 HSI Applications in Air Quality Monitoring

#### 4. Applications of HSI in Water Quality Monitoring

HSI helps identify pollutants and contaminants in water bodies that are invisible to the naked eye. By examining spectral patterns, it can effectively map and measure the pollution level including detecting harmful algal blooms and identifying toxic substances. Additionally, HSI facilitates the early detection of pollution trends, offering valuable insights for management and improving the accuracy of water quality assessments. Jiang, Q., et al., examined the feasibility of visible and NIR spectroscopy (VNIRS) with 103 samples using ASD FieldSpec3 spectral radiometer (Analytical Spectral Devices), wavelength of 400-2350 nm, obtaining  $r^2_{CV}$  ranging from 0.32 and 0.40, a Partial Least Square Regression (PLSR) with a Genetic Algorithm (GA) and Competitive Adaptive Reweighted Sampling (CARS) increases heavy metals monitoring [104]. A technique of remote sensing for UAV-HSI for urban water pollution sources has been developed by Cai, X., et al., using 3D Excitation-Emission Matrix Fluorescence Spectroscopy, a Ubert ultrahigh definition (UHD) 185-Firefly hyperspectral camera collected 125 bands ranging 450-950 nm with the spatial and spectral resolution of 4 nm and 0.06 m respectively, the dataset analyzed had 337 polluted water samples, achieved

a recognition accuracy (RA) of 71.43%, and concentration of Chl-a with RMSE of 6.87 µg/L and 17.58% of mean absolute percentage error (MAPE) recognized as better performance [105]. Pan, X., et al., proposed a method to show that the quality of offshore seawater measuring can be effectively performed by UAVs and airborne hyperspectral remote sensing (HRS) technology, mainly focusing on Chl-a and total suspended matter (TSM) concentrations using data from 30 water samples, the training model achieved an accuracy of R<sup>2</sup> in (0.712 for Chl) and (0.756 for TSM) with relative percentage difference (RPD) of 3.72 and 5.83, the Rp<sup>2</sup> values of both are greater than 0.7 resulting high prediction [106]. Leung, J.-H., et al., developed a method for quantifying water pollutants through spectral analysis by identifying the images of biological oxygen demand (BOD) captured through 3D-CNN with 2,545 images achieving an accuracy of 80%, with the spectral data of 40 nm, achieving an 8% increase in the accuracy of the Good category in F1-score [107]. A real-time hyperspectral underwater detection based on BS was proposed by Fu, X., et al., using hyperspectral digital imagery collection experiment (HYDICE) data having 169 spectral bands and 1.56 m of spatial resolution, and HSI including 256 bands in the 0.4–1.05 nm in the spectral region, using Constrained-Target Optimum Index Factor Band Selection (CTOIFBS) and Constrained Energy Minimization (CEM) algorithm, evaluating using receiver operating characteristic (ROC) [108]. Riaza, A., et al., developed a method using hyperspectral remote sensing (HyMap) of spectral range (436-2485) nm and resolution (0–20) nm to map the polluted river water with ASD FieldSpec3 spectrometer ranging from 400-2400 nm at 1 nm spectral resolution to achieve high-resolution maps with 4 m [109]. The joint framework for underwater hyperspectral image restoration and target detection (JURTD) module was developed by Li, Q., et al., enabling high-quality images with superior detection of pollutants using GaiaField Portable spectral imager with a spectral resolution of 2.8 nm across the wavelength of 400 nm to 1000 nm with 120 spectral bands, evaluating using the PSNR, spectral angle mapper (SAM) and structural similarity index (SSIM) for restoration, receiver operating characteristic (ROC) curves and area under the curve (AUC) values were utilized for the detection [110]. Hough, I.M., developed a novel and adaptable framework using the hydro-ecological model in Sedimentation and River Hydraulics (SRH-2D) and the Computer Aided Simulation Model for Instream Flow and Riparia (CASiMiR), improvements in Hydraulic Habitat Suitability (HHS) ranging 0.5–0.6 and enhancing peak species habitat qualities by 23–26% while reducing water usage by 22% [111]. Qi, J., et al., proposed a self-improving underwater target detection framework (SUTDF) using deep learning with a range of 400-1000 nm and spectral resolution of 2.22 nm for lake water and 366-2495 nm at 9.5 nm for seawater with superior detection performance with an AUC value of 0.945 in military/civilian applications [112]. Yuan, A., et al., developed a cost-effective portable edge AI system with an Algal Morphology Deep Neural Network

(AMDNN) model for the detection of algae and harmful algal blooms (HAB) using NVIDIA Jetson TX1 chip with a range 10-1000 and 50-1400 pixels, with an accuracy of 99.87% in HAB early warning applications and fisheries [113]. UAV-HSI data combined with the SpectralFormer model for the aquatic plant classification proposed by Yu, Z., et al., using high-resolution imagery captured at 100m with 0.1m of spatial resolution using the Pika L imaging spectrometer, achieving 93.15% in overall accuracy (OA), 89.14% in a Kappa coefficient, and 84.55% in a mean IoU with a range of 700-1000 nm, by improving the models such as SegNet, Deeplabv3+, and HSI-TransUNet by 3.11% for Kappa and 2.91% for mIoU [114].

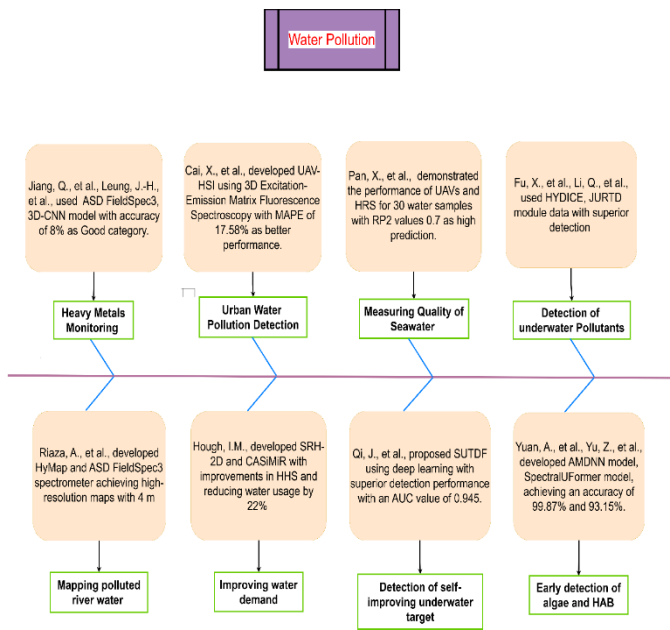


Fig. 3 HSI Applications in Water Quality Monitoring

### 5. Applications of HSI in Soil and Vegetation Monitoring

HSI in soil monitoring can identify changes in soil moisture, composition, and texture, which are crucial for evaluating soil health and fertility. In vegetation, monitoring plant health by early identification of disease, stress, or nutrient deficiency through variations in leaf reflectance. By examining the spectral data, HSI can map the vegetation cover, species distribution, and growth patterns, providing valuable insights into agricultural productivity, ecosystem health, and real-time information on soil and vegetation. Furlanetto, R.H., et al., proposed a hyperspectral method for early detection of potassium (K+) deficiency in soybean detection, using PCA and linear discriminant analysis (LDA) in an ASD Fieldspec 3 Jr. hyperspectral sensor to collect spectral data, generating 3024 samples from 252 reflectance spectra with the range of 400–1000 nm, with 3 nm of resolution, LDA achieved an accuracy of more than 70% and 59% for simulation and validation, with performance evaluation of 70-30% split for

training and testing [115]. Banerjee, B.P., et al. proposed a UAV-HSI framework to identify challenges of the data acquisition, sensor calibration, mosaicking, illumination correction, and geometric alignment for environment monitoring, capturing of images with a resolution of 1024 × 1024 in 15 bands in the 500–900 nm spectral range, having a geometric accuracy with an absolute RMSE of 5.43cm with a standard deviation of 4.24 cm and a SAM of 0.086 rad, high-precision indices including the Vogelmann index (VOG) and a red edge (RE) validated, with SMAPE values of 8.9% and 17.2% [116]. Ferral, A., et al., combined satellites with nanotechnology to avoid pollution and climate change, using LANDSAT, Sentinel, and hyperspectral satellite missions such as PRISMA, EnMAP, and PACE by collecting more than 100 spectral bands each having a width of 10–20nm [117]. Dimobe, K., et al., examined the drivers of land degradation and deforestation (LDD) in the Total Wildlife Reserve of Bontoli (TWRB) using advanced remote sensing and geographical information system (GIS) analysis for detection of land use and land cover (LULC) changes by employing Landsat images such as Thematic Mapper (TM), Enhanced Thematic Mapper (ETM+), and Operational Land Imager–Thermal InfraRed Sensor (OLI–TIRS) with 30m resolution, achieving an OA with a kappa coefficient exceeding 85% using maximum likelihood classification (MLC) algorithm for mapping and analysis [118]. Mao, D., et al., applied different techniques of Surface Energy Balance Algorithm for Land (SEBAL) and Integrated Valuation of Ecosystem Services and Trade-offs (InVEST) by integrating remote sensing, statistical data, and meteorological records to estimate effect on land cover and ecosystem services, verifying 256 Landsat TM/ETMp and 289 Landsat OLI scenes, the OA in land cover classification was 92% and 94%, use of water yield reduce by 11.8% and sandstorm prevention increased by 1.3% [119]. An 18-class LULC classification approach was expertized by Feng, S., et al., by enabling detailed and reliable data for the monitoring and analysis of ecosystem changes at the level of a basin using images taken by Sentinel-2 to obtain data from the Google Earth Engine (GEE) system that was used in the RF algorithms with a 10 m spatial resolution by integrating the Shuttle Radar Topography Mission (SRTM) model on the GEE platform with a spatial resolution of 30 m achieving a OA of LULC maps ranging 87.45% and 93.02% [120]. Thangavel, K., et al., proposed another method using an automated system for wildfire detection using HSI and a 1D-CNN that was reliable enough for ecosystem monitoring at the basin scale using PRISMA satellite data with a 5m resolution and 30m of spatial resolution spectrometer covering 400-2505 nm spectral bands, achieving real-time data processing with a dataset split of 70% for training and 30% for validation and enable trusted autonomous satellite operations (TASO) for early fire detection and risk mapping to support disaster management [121]. The enhancement of imaging spectrometers for vegetation mapping in forest environments through simulations was introduced by Chaity, M.D. and J. van Aardt, using Digital Imaging and

remote sensing Image Generation (DIRSIG) technology, achieving OA of 84% with high-resolution configurations such as ground sampling distances of 1 m and 3 nm resolutions ranging from 380–2510 nm using 1D-CNN for accurate species identification [122]. Brook, A., et al., proposed a multiscale equipped with CNN for the pan-sharpening of Sentinel-2A images with 10 m of spatial resolution using UAV images to examine plant responses, and evaluated using the QNR index of 0.87, Ds spatial component of 0.11, and a Dλ spectral component of 0.08 with spectral regions >800 nm supports best results, DJI Phantom 4 Pro Quadcopter has 12.4 million pixels, a compact field spectrometer OceanOptics USB4000, and NIR-FLAME ranges from 350–1800 nm with a 0.5 nm bandwidth [123]. Mäyrä, J., et al., examined the execution of a 3D-CNN in combination with an artificial neural network (ANN), support vector machine (SVM), RF, and gradient boosting machine for the species classification with high-resolution hyperspectral data and LiDAR with 0.5 m of spatial resolution, an altitude of 1500 m, achieving a spectral range of VNIR (406–995 nm) and SWIR (956–2525 nm), with the 3D-CNNs achieving F1-score of 0.91 for aspen, 87% of OA and in ANN (0.86) of OA [124].

spectral range and 15 nm of resolution and an image resolution of 128 × 128 pixels, which is used in fruit quality, tooth color determination, and volcanic rock mineralogy applications [125]. To obtain precise spectral details from mm-scale spatial regions Stuart, M.B., et al., introduced a semi-portable, cost-effective, and high-resolution HSI that utilized Canon EF-S lens, Edmund Optics diffraction grating, and a Hamamatsu imaging sensor ranging from 450 nm to 650 nm and 0.29 nm of spectral resolution, and 1000 pixel in spatial resolution applied on various applications including mining, environmental monitoring, petrology, and geological exploration, etc [126]. A systematic image mosaicking method for environmental monitoring was introduced by Yi, L., et al., using ZK-VNIR-FPG480 HSI equipped with a DJI M600 Pro UAV with a medium error of 1.76m in the river course area and 1.9669 m in the forest area, SIFT and RANSAC achieved good results ranging from 400–1000 nm and 2.8 nm of spectral resolution in 270 bands applied on applications such as mineral exploration, water monitoring, and forestry analysis [127]. Horstrand, P., et al., proposed a method using HSI in a commercial DJI Matrice 600 drone and a Specim FX10 hyperspectral camera capturing 224 spectral bands ranging from 400–1000 nm and used a HyperLCA compressor to perform real-time data acquisition greater than 300 FPS, which is applied in applications including target tracking, mining, environmental monitoring, and remote sensing [128]. An advanced mineral classification system developed by Radulescu, M., et al., utilizing machine learning algorithms to integrate data using the EfficientDet architecture and FinTech solution that enabled deep learning with a high accuracy of 98% in laboratory spectra ranging from 450–950 nm and 1650–160 mm [129]. Integrating of NIR HSI and DCNN techniques used by Nie, P., et al., focused on identifying hybrid seeds using 200 broad bands within the 780–2500 nm range, the discriminant analysis models used PLS Discriminant Analysis (PLS-DA), SVM, and DCNN, among all the models DCNN was highly stable and achieved a classification precision of more than 95% [130]. Ahmed, M.T., has proposed a low-cost and quality assessment tool for biological and agricultural applications using deep learning based on HSI reconstruction with 204 spectral bands with a range of 400–1000 nm and 7 nm spectral resolution, High-resolution network (HRNET) provides higher performance by achieving the lowest mean relative absolute error (MRAE) of 0.07, the root MSE of 0.03, and the high PSNR of 32.99 dB [131]. A system that estimates crop yield and biomass was developed by Li, K.-Y., et al., using R and Python, an auto-generated hyperspectral narrowband vegetation index calculations and advanced AutoML technology uses 216 spectral bands with a range of 409-989 nm and 2.69 nm of spectral resolution achieving the best R<sup>2</sup> of 0.96 and NRMSE of 0.12 [132]. A Mobile LiDAR Systems (MLS) approach based on open-pit mining was introduced by Wajs, J., et al., for a Riegl VMZ 400i measurement platform and a Velodyne LiDAR sensor in the Simultaneous Localization and Mapping (SLAM) method to collect data and localize within a

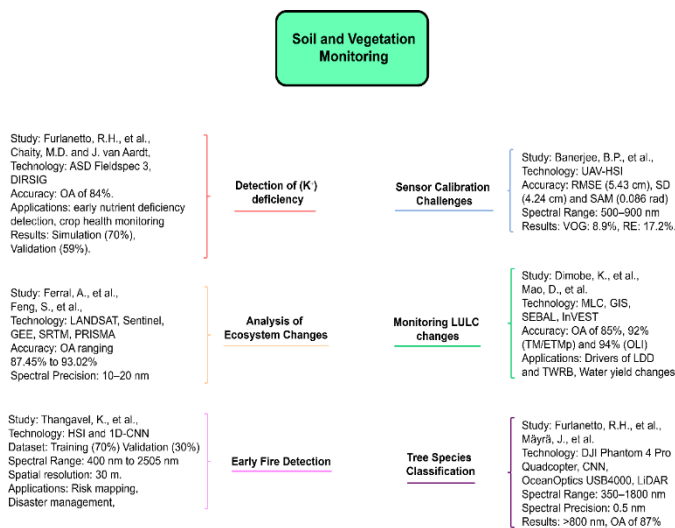


Fig. 4 HSI Applications in Soil and Vegetation Monitoring

## 6. Technological Advances in HSI for Environmental Sensing

Recent advancements in HSI for environmental sensing have enhanced the data collection. It captures a broad range of light, allowing for the identification of spectral differences in pollutants. Technological advances are concentrating on making hyperspectral sensors portable and affordable, which is used in drones, and satellites. Improvements in sensor calibration and data fusion techniques have enhanced the accuracy and reliability of environmental models. Stuart, M.B., et al., proposed a low-cost HSI for laboratory purposes using a miniature spectrometer, rotary mirror setup, and Thorlabs Plano-convex lens with >97% reflectance, 340-850 nm of

range of 800 m achieving an accuracy of  $\pm 5$  cm using the SLAM-based method [133]. Yang, G., et al., developed an Enhanced Mangrove Vegetation Index (EMVI) using an HSI approach for a fast and accurate mangrove mapping by using data from ZY1-02D, GF-5, Hyperion, and PRISMA satellites, focusing on the spectral bands including Green (533 nm), SWIR1 (1660 nm), and SWIR2 (2200 nm), and the classification have achieved an OA of greater than 90%, which shows the high precision of EMVI in the SVM model [134]. Zhao, G., et al., presented a novel dual-branch method for vehicle trajectory using Light Detection and Ranging (LiDAR), an Inertial Measurement Unit (IMU), a monocular camera, and GPS to improve joint classification by combining multisource heterogeneous data with HSI analysis with a range of 0.38 to 1.05  $\mu\text{m}$  applied in applications including precision agriculture, semantic segmentation, and urban planning [135]. Zhang, M., et al., implemented the Structural Optimization Transmission Network (SOT-Net) for land-cover classification using HSI data and LiDAR classification ranging between 0.38 and 1.05  $\mu\text{m}$  obtaining an OA of 91.17% in GSOT, it is applied to applications including environmental monitoring, forest management, and earth observation [136].

increase in spatial resolution. Advanced data processing techniques and high-resolution sensors have enabled improved image clarity, detailed spatial information, and precision by enhancing the capabilities of environmental monitoring.

The spatial resolution limitation that was previously present at the meter level can be overcome using long-distance sensing and high-resolution as well as trade-off factors in distributed optical fiber sensors (DOFSs) according to Guo, Z., et al., who have found that these factors contribute to both high accuracy and enhanced temporal and spatial response [137]. The Visible Infrared Imaging Radiometer Suite Day/Night Band sensor and astronaut photographs have recently been developed by McIsaac, M.A., et al., with a spatial resolution higher than the satellite-based observations for air pollutant concentrations [138]. Carle, M.V., et al., used a commercial high spatial resolution WorldView-2 (WV-2) satellite launched by DigitalGlobe, which contributed 2 m imagery, applied MLC and SVM classification to map freshwater to overcome the issue of using only 4 m spatially resolved HyMap data to map small river paths [139]. A low-cost, freely available satellite-based IS imagery is used for species identification having a low spatial resolution to overcome this limitation, cloud-free mosaics of improved imagery have been developed by Helmer, E.H. and B. Ruefenacht, for time-lapse images, a regression tree used to estimate the digital numbers (DNs) under clouds and cloud shadows in a Landsat image from a cloud-free area, and the image adjacent the cloud-free image is matched through a histogram based on the corresponding area [140]. By reconstructing a module with multiple bands and using Fourier transform upsampling Bu, L., et al., overcame the limitations of space-borne hyperspectral technologies and achieved a high-resolution hyperspectral image that includes global information [141].

## 7.2 Cost

HSI is expensive because of specialized sensors, optics, high-resolution detectors, and equipment being used. The process of integrating HSI systems into aerial platforms/drones requires high deployment and maintenance costs. New approaches have been focused on developing low-cost alternatives that would utilize cloud computing for storage and data processing in a scalable and efficient way. Handling large datasets and reducing computational cost, achieving through the use of distributed processing algorithms. Cost-effective sensors and microfluidic devices can offer precise measurements.

The cost of IFCB and FlowCAM instruments is too high which is why Reale, R., et al., developed a simple and inexpensive system that uses microfluidic scanning flow cytometer ( $\mu\text{SFC}$ ) measurements, angle-resolved scattering light can provide accurate and quantitative estimates of cellular properties [142]. To overcome the limitations of comparable computation resources of HSI across increasing camera numbers, Zheng, P., et al., discovered cloud computing as a promising solution for

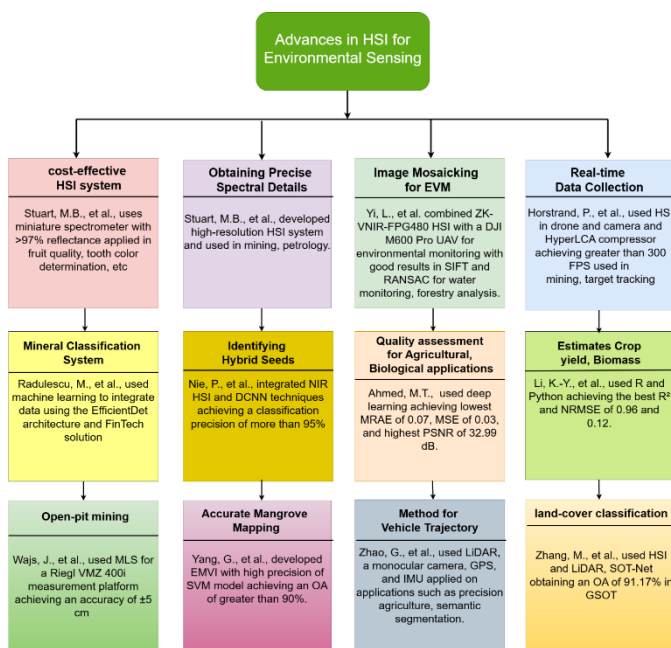


Fig. 5 HSI Advancements for Environmental Sensing

## 7. Challenges and Future Directions

### 7.1 Spatial resolution

Despite HSI being an essential technique for monitoring environmental factors such as vegetation health, water quality, and pollution levels, the limitations in spatial resolution have been challenging due to its inability to capture fine details over large areas which makes it difficult to distinguish variations which is essential for accurate analysis. The development of sensors and imaging mechanisms has led to a significant

HSI storage and processing utilizing Spark, which can be scalable for storage capacity and provide high-performance computing power, as well as employ distributed parallel unmixing algorithms including parallel pixel purity index (PPI) and sum-to-one constrained least squares (SCLS) [143]. Using HSI instruments is limited to research laboratories because of the high cost of collecting data from airborne platforms therefore, Stuart, M.B., et al., have introduced a Low-Cost High-Resolution HSI for monitoring by enabling an important area for further development [126]. Due to computational complexity, mathematical optimization techniques and manifold learning make solving processes challenging when dealing with large datasets that must be eliminated to overcome, Yi, W., et al., demonstrate the use of Uniform Manifold Approximation and Projection (UMAP) as a cost-effective function for obtaining arbitrary fuzzy topological structures in high-dimensions [144]. Interband redundancy analysis (IBRA) removes redundant bands by decreasing the search space within a feature extraction framework developed by Morales, G., et al., using Dimensionality reduction techniques to reduce the spectral bands to address the limitation of spectral channels in HSI [145].

### 7.3 Dataset

The limitations of datasets including missing data, a lack of labeled samples, and imbalanced class distributions pose a major challenge to the performance of models and their accuracy. To overcome these issues, it is essential to utilize advanced technology and innovative approaches such as data generation, transfer learning, and data augmentation.

To overcome the disadvantage of approximately 1% of the dataset's missing data, Ambler, G., et al., applied hotdecking for incomplete data, which involves sampling and replacing observed data and matching can reduce biased regression estimates. Additionally, Multiple Imputation by Chained Equations (MICE) is used, which is assigned with missing data based on the conditional density of each predictor that is best performing [146]. The limitation of collecting only a small number of labeling samples in practice is overcome by the model discovered by Lighthart, A., et al., that self-training is best out of 4 semi-supervised models that outperform traditional supervised models when data is limited as it can reduce labeling data by maintaining high performance which is useful in retrieving labeled data [147]. Common hyperspectral datasets have a limited number of labeled training samples to overcome the limitation Ahmad, M., et al., introduced an MLR-based classifier for high-dimensional multi-class HSI data, which actively selects data based on the sample's fuzziness and non-randomized selection of samples to be random [148]. Utilizing two distinct datasets, a simulated spatiotemporal field and an actual dataset of temperature measurements requires more storage capacity to overcome this da Silva, L.A., et al., implemented GAN to address the issue of imbalanced data in the manufacturing domain such as videos [149]. Combining

spectral and visible images from various sensors, Kizel, F. and J.A. Benediktsson, proposed a methodology that uses IPs for radiometric calibration of RGB values before processing them with spatial features-aided neural network (SFANN) data to improve resolution and accurate representation of tree species to map in complex forests [150]. Previous observations have hindered the early results of river channel acid water mapping, using satellite images proposed by Wu, T., et al., can overcome this disadvantage by combining modified normalized difference water index (MNDWI) and Otsu's feature to extract the channel centerlines using water mask maps and RivWidthCloud providing high temporal resolution and global coverage [151].

### 7.4 Spectrometer

The spectrometer is used for environmental monitoring, material evaluation, and atmospheric research but, the instruments are not effective because of some limitations like environmental sensitivity that changes measurements and calibration. The complexity of data processing generates a huge amount of data. Technological advancements have focused on both hardware and software which has led to more robust calibration methods, application of advanced algorithms for more efficient data analysis, and designing high-sensitive sensors that can operate in a wide range of environments.

Airborne HSI could not calibrate with rigorous spectroradiometric, as artifacts affect the best-behaved instruments to overcome this limitation Jia, G., et al., have recently demonstrated an Airborne Prism Experiment (APEX), and a center wavelength (CWL) shift that aims to minimize pressure, temperature, and vibrations during flight operations and calibration using atmospheric absorption features and characteristics from standardized reference material filters within the APEX in-flight characterization facility [152]. The measurement of air pollution in a designated area by drone scanning is problematic, as the single-flight capacity is outweighed by the task area to overcome this disadvantage, Baumgart, J., integrated the Carthaginian War Elephant Swarm Optimization (CWESO) algorithm, air pollution is monitored and analyzed by drones by adapting variability in the wind with the addition of supplementary scout drone to explore their surroundings and coordinate the entire team [153]. The limitations of the underwater spectral imaging system employing electric filter wheels to capture single-band images in various bands have been overcome by Song, H., et al., who designed a Liquid Crystal Tunable Filter (LCTF) that is a compact and minimally constructed optical geometry, so it can rapidly generate high-quality spectra by arbitrarily switching between various spherical bands for reliable spectral image data [154]. To overcome the challenges related to the accuracy of the input cross-section and the same absorption bands, Zhou, J., et al., developed mid-infrared (mid-IR) silicon nitride (SiN) waveguides sensor outlined and examined for VOC detection to perform on-chip mid-IR spectral measurements [155]. For

the identification of pollutants, HSI sensors are necessary to have >100 spectral bands between 10–20 nm, and other systems range from 500–900 nm with >10 nm resolution and spectra at 1 nm to overcome this drawback, Xiao, Y., et al., developed high-resolution lidar technique that allows accurate retrieval of extinction and transmission through narrower spectral filters to differentiate between molecular and particulate backscattering patterns [156]. Many spectral bands form a complex structure for data to overcome this limitation, Zhang, L., et al., used the BS method to decrease the cost and computational complexity of HSI in the spectral region [157]. Fan, S., et al., utilized the spectral data from spectroscopic techniques by analyzing the feature selection method, PLS-DA, and SVM combined with data level, decision level, and feature level, achieving better classification and overcoming the issue of GaiaField Hyperspectrometer ranging from 400-1000 nm and 2.8 nm of spectral resolution [158].

## 7.5 Band determination

The development of robust band-determination methods is required to overcome challenges such as overlapping spectral bands, background noise, and huge amounts of information, requiring appropriate analysis and modeling frameworks to provide more accurate predictive analyses and optimize data interpretation. Many studies have proposed new methods to overcome these limitations using machine learning, statistical models, and hybrid approaches to select spectral bands for specific applications.

The instrument's limitation of the magnitude of background noise and the similar absorption and composition of VOC species pose significant challenges to accurate VOC detection. Zatta, D., et al., proton transfer reaction-mass spectrometry (PTR-MS) can overcome these challenges to enable VOC detection with higher time resolution, approximately ten seconds/minute for quadrupole mass analyzers and almost instantaneous for time-of-flight mass analyzers [159]. WResVLM, a semi-supervised learning framework that employs vision-language models (VLMs) to restore images in diverse weather conditions, has been developed by Xu, J., et al. to overcome the disadvantage of air pollution caused by low light levels during adverse weather events. The technique evaluates the images using VLM and selects pseudo-labels to train the restoration model by applying prompt learning to adapt the VLM for modifying the restoration process. The framework addresses the domain gap between real and synthetic data during early training stages by combining existing image restoration techniques with the proposed VLM evaluation and gradually updating pseudo-labels, and weather prompts to maximize performance [160]. The limitation of the nonspecific and multi-collinear nature of Soil VNIR spectra due to redundant noise and spectral overlap hinders its ability to predict soil properties accurately to overcome this, Laamrani, A., et al., introduced a multimethod modeling

approach that utilizes Random Forest, SVM, and PLSR models for band selection and to examine the selected bands by identifying optimal bands within the VNIR and SWIR spectral ranges that are sensitive to Soil Organic Carbon (SOC) and useful for mapping by providing a new framework for developing sensors designed for SOC detecting [161]. BS techniques are incorporated into terrestrial HTD techniques for detecting underwater targets, which rely on appropriate BS techniques to select band subnets with spectral wavelengths that connect to the target of interest by lowering the size of the dataset to overcome this limitation, Song, M., et al., adopted the virtual measurement (VD) method to determine the number of unsupervised clusters to overcome the minimum evaluation of band sets, the local optimal solution of the multi-objective development algorithm [162].

## 7.6 Hardware complexity

HSI technology faces severe challenges because of hardware complexity, including sensor design, energy efficiency issues, and high manufacturing costs. These limitations restrict the widespread use of HSI in expert research. Using of advanced technology can overcome these problems through improved system design, lightweight components, and the refinement of measurement techniques by increasing data accuracy and efficiency.

Sensor design and storage capacity limitation can be overcome by implementing sensor node architectures by Lopriore, L., who posed significant challenges in terms of hardware complexity and energy consumption, limits the use of highly complex devices like memory management units for virtual-to-physical address translation. An interface for protection hardware is formed inside the microcontroller, the memory protection unit (MPU), interposed between the processor and the memory devices consisting of primitives called protection operations. To ensure memory separation between tasks, the compiler inserts the calls to these operations at specific locations within the object code while keeping the application programmer from explicitly calling them [163]. The use of HSI instruments is restricted to research laboratories because of weight and high cost to overcome this limitation, Guo, T., et al., implemented spectral resolution that is primarily determined by the quality of an optical path and the thickness of one grating in the prism for spectrum capture, as well as the mechanical scanning component for image acquisition [164]. The limitation of weak scattering sunlight at 200-350 nm, using the blackbody calibration down to 200 m used by Thuillier, G., et al., is necessary for the enhancement of the UV light signal rather than simply combining the deuterium lamp and black beam for the SL1 instrument for absolute calibration. The utilization of a double monochromator with holographic gratings greatly minimizes scattered light, making UV measurements more effective [165]. SCanning Imaging Absorption Spectrometer for Atmospheric CHartographyY

(SCIAMACHY) is a passive instrument to overcome this limitation, Shea, Y.L., et al., discovered that Earth-reflected radiation from SCIAMACHY for atmospheric reflectance over large spatial scales is advantageous for studying climate change achieved by changing Shannon entropy across different instruments and scale [166].

## 8. Conclusion

In conclusion, HSI in environmental sensing has been enhanced by technological advancements. The development of imaging techniques has enabled to obtain data with greater accuracy, and machine learning models have been introduced to improve the interpretation of large datasets. The advancement in portable and cost-effective technology has enabled HSI to be integrated with drones and satellites, making it more suitable for remote and large-scale monitoring. By combining AI, IoT, and sensor systems, HSI can offer significant progress. In future developments, spatial resolution should be improved. HSI can enhance model performance by incorporating multi-modal datasets and deep learning algorithms. Low-cost and rapid small-scale sensors offer substantial potential for decentralized monitoring. Additionally, implementing cloud-based solutions and collaborative data fusion techniques can facilitate the establishment of sustainable environmental management strategies. HSI can be instrumental in environmental monitoring by providing valuable insights to monitor climate change, biodiversity loss, and pollution. The future is promising, with a lot of potential to contribute to sustainable development and environmental preservation.

## REFERENCES

- Zamora-Polo, F., et al., *What do university students know about sustainable development goals? A realistic approach to the reception of this UN program amongst the youth population*. Sustainability, 2019. **11**(13): p. 3533.
- Miyazawa, I., *What are Sustainable Development Goals?* 2012: JSTOR.
- Costanza, R., et al., *Modelling and measuring sustainable wellbeing in connection with the UN Sustainable Development Goals*. Ecological economics, 2016. **130**: p. 350-355.
- Bigot, S., et al., *Pivotal roles of environmental sensing and signaling mechanisms in plant responses to climate change*. Global change biology, 2018. **24**(12): p. 5573-5589.
- Andres, L., et al., *A review of in-situ and remote sensing technologies to monitor water and sanitation interventions*. Water, 2018. **10**(6): p. 756.
- Borah, S.S., A. Khanal, and P. Sundaravadivel, *Emerging Technologies for Automation in Environmental Sensing*. Applied Sciences, 2024. **14**(8): p. 3531.
- Chung, C.-c. and T.-s. Jeng, *A Citizen-Sensing System for Measuring Urban Environmental Quality: A Case Study Carried out in Taiwan*. Applied Sciences, 2022. **12**(24): p. 12691.
- Kays, R., et al., *Terrestrial animal tracking as an eye on life and planet*. Science, 2015. **348**(6240): p. aaa2478.
- Chen, C.-W., et al., *Air pollution: Sensitive detection of PM<sub>2.5</sub> and PM<sub>10</sub> concentration using hyperspectral imaging*. Applied Sciences, 2021. **11**(10): p. 4543.
- Chao, L., et al., *Particulate matter and inflammatory skin diseases: From epidemiological and mechanistic studies*. Science of The Total Environment, 2023: p. 167111.
- Chowdhury, S., et al., *Changing risk factors that contribute to premature mortality from ambient air pollution between 2000 and 2015*. Environmental Research Letters, 2020. **15**(7): p. 074010.
- Van Donkelaar, A., et al., *Use of satellite observations for long-term exposure assessment of global concentrations of fine particulate matter*. Environmental health perspectives, 2015. **123**(2): p. 135-143.
- Alfano, B., et al., *A review of low-cost particulate matter sensors from the developers' perspectives*. Sensors, 2020. **20**(23): p. 6819.
- Liang, Y., et al., *Study of the Composite Oscillator of Particulate Monitoring Instrument Based on TEOM*. Applied Mechanics and Materials, 2014. **678**: p. 274-280.
- Chan, S. and Y. He, *Measurements of particulate mass concentration using a tapered-element oscillating microbalance and a flame ionization detector*. Measurement Science and Technology, 1999. **10**(4): p. 323.
- Schwab, J.J., et al., *Laboratory characterization of modified tapered element oscillating microbalance samplers*. Journal of the Air & Waste Management Association, 2004. **54**(10): p. 1254-1263.
- Kinsey, J.S., et al., *Evaluation of methods for the determination of diesel-generated fine particulate matter: Physical characterization results*. Journal of aerosol science, 2006. **37**(1): p. 63-87.
- Kang, C.-K., *Neural network modeling of particulate matter concentration in the Golden Triangle area*. 2003: Lamar University-Beaumont.
- Schwarzenbach, R.P., et al., *Global water pollution and human health*. Annual review of environment and resources, 2010. **35**(1): p. 109-136.
- Lin, L., H. Yang, and X. Xu, *Effects of water pollution on human health and disease heterogeneity: a review*. Frontiers in environmental science, 2022. **10**: p. 880246.
- Zhang, Y., et al., *Retrieval of water quality parameters from hyperspectral images using hybrid Bayesian probabilistic neural network*. Remote Sensing, 2020. **12**(10): p. 1567.
- Vasudevan, S.K. and B. Baskaran, *An improved real-time water quality monitoring embedded system with IoT on unmanned surface vehicle*. Ecological Informatics, 2021. **65**: p. 101421.
- Murphy, K., et al., *A low-cost autonomous optical sensor for water quality monitoring*. Talanta, 2015. **132**: p. 520-527.
- Tang, Y., et al., *Active and low-cost hyperspectral imaging for the spectral analysis of a low-light environment*. Sensors, 2023. **23**(3): p. 1437.
- Attivissimo, F., et al., *A portable optical sensor for sea quality monitoring*. IEEE Sensors Journal, 2014. **15**(1): p. 146-153.
- Akinawo, S.O., *Eutrophication: Causes, consequences, physical, chemical and biological techniques for mitigation strategies*. Environmental Challenges, 2023. **12**: p. 100733.
- Yeh, P., et al., *Applications of LEDs in optical sensors and chemical sensing device for detection of biochemicals, heavy metals, and environmental nutrients*. Renewable and Sustainable Energy Reviews, 2017. **75**: p. 461-468.
- Li, Z., D. Xu, and X. Guo, *Remote sensing of ecosystem health: opportunities, challenges, and future perspectives*. Sensors, 2014. **14**(11): p. 21117-21139.
- Jupp, D.L., J.T. Kirk, and G.P. Harris, *Detection, identification and mapping of cyanobacteria—using remote sensing to measure the optical quality of turbid inland waters*. Marine and Freshwater Research, 1994. **45**(5): p. 801-828.
- Chang, N.-B., S. Imen, and B. Vannah, *Remote sensing for monitoring surface water quality status and ecosystem state in relation to the nutrient cycle: a 40-year perspective*.

- Critical Reviews in Environmental Science and Technology, 2015. **45**(2): p. 101-166.
31. Gholizadeh, M.H., A.M. Melesse, and L. Reddi, *A comprehensive review on water quality parameters estimation using remote sensing techniques*. Sensors, 2016. **16**(8): p. 1298.
  32. Sivathanu, Y., *Natural gas leak detection in pipelines*. Technology Status Report, En'Urga Inc., West Lafayette, IN, 2003.
  33. Saha, D. and A. Manickavasagan, *Machine learning techniques for analysis of hyperspectral images to determine quality of food products: A review*. Current Research in Food Science, 2021. **4**: p. 28-44.
  34. Stuart, M.B., A.J. McGonigle, and J.R. Willmott, *Hyperspectral imaging in environmental monitoring: A review of recent developments and technological advances in compact field deployable systems*. Sensors, 2019. **19**(14): p. 3071.
  35. Manley, M., *Near-infrared spectroscopy and hyperspectral imaging: non-destructive analysis of biological materials*. Chemical Society Reviews, 2014. **43**(24): p. 8200-8214.
  36. Zahra, A., et al., *Current advances in imaging spectroscopy and its state-of-the-art applications*. Expert Systems with Applications, 2024. **238**: p. 122172.
  37. Jamme, F. and L. Duponchel, *Neighbouring pixel data augmentation: a simple way to fuse spectral and spatial information for hyperspectral imaging data analysis*. Journal of Chemometrics, 2017. **31**(5): p. e2882.
  38. Zabalza, J., et al., *Novel two-dimensional singular spectrum analysis for effective feature extraction and data classification in hyperspectral imaging*. IEEE transactions on geoscience and remote sensing, 2015. **53**(8): p. 4418-4433.
  39. ElMasry, G. and D.-W. Sun, *Principles of hyperspectral imaging technology*, in *Hyperspectral imaging for food quality analysis and control*. 2010, Elsevier. p. 3-43.
  40. Khan, M.J., et al., *Modern trends in hyperspectral image analysis: A review*. Ieee Access, 2018. **6**: p. 14118-14129.
  41. Jones, C., et al., *Understanding multispectral imaging of cultural heritage: Determining best practice in MSI analysis of historical artefacts*. Journal of Cultural Heritage, 2020. **45**: p. 339-350.
  42. Nowak, P.M. and P. Kościelniak, *What color is your method? Adaptation of the RGB additive color model to analytical method evaluation*. Analytical chemistry, 2019. **91**(16): p. 10343-10352.
  43. Asner, G.P., et al., *Carnegie airborne observatory: in-flight fusion of hyperspectral imaging and waveform light detection and ranging for three-dimensional studies of ecosystems*. Journal of Applied Remote Sensing, 2007. **1**(1): p. 013536.
  44. Mateen, M., J. Wen, and M.A. Akbar, *The role of hyperspectral imaging: A literature review*. International Journal of Advanced Computer Science and Applications, 2018. **9**(8).
  45. Bhargava, A., et al., *Hyperspectral Imaging and Its Applications: A Review*. Heliyon, 2024. **10**(12).
  46. Yu, L., et al., *Monitoring surface mining belts using multiple remote sensing datasets: A global perspective*. Ore Geology Reviews, 2018. **101**: p. 675-687.
  47. Lodhi, V., D. Chakravarty, and P. Mitra, *Hyperspectral imaging system: Development aspects and recent trends*. Sensing and Imaging, 2019. **20**: p. 1-24.
  48. Gondek, J.S., G.W. Meyer, and J.G. Newman, *Wavelength dependent reflectance functions*. in *Proceedings of the 21st annual conference on Computer graphics and interactive techniques*. 1994.
  49. Villarroel, M., et al., *Direct esthetic restorations based on translucency and opacity of composite resins*. Journal of Esthetic and Restorative Dentistry, 2011. **23**(2): p. 73-87.
  50. Durmus, D., *Optimising light source spectrum to reduce the energy absorbed by objects*. 2017.
  51. Siche, R., et al., *Evaluation of food quality and safety with hyperspectral imaging (HSI)*. Food Engineering Reviews, 2016. **8**: p. 306-322.
  52. Shaw, G.A. and H.K. Burke, *Spectral imaging for remote sensing*. Lincoln laboratory journal, 2003. **14**(1): p. 3-28.
  53. Soukup, M., et al., *HYPERCUBE: ONBOARD PROCESSING OF HYPERSPECTRAL IMAGING DATA ON A NANOSATELLITE*. 2016.
  54. Qi, Y., et al., *Recent progresses in machine learning assisted Raman spectroscopy*. Advanced Optical Materials, 2023. **11**(14): p. 2203104.
  55. Hasan, B.M.S. and A.M. Abdulazeez, *A review of principal component analysis algorithm for dimensionality reduction*. Journal of Soft Computing and Data Mining, 2021. **2**(1): p. 20-30.
  56. Caggiano, A., et al., *Dimensionality reduction of sensorial features by principal component analysis for ANN machine learning in tool condition monitoring of CFRP drilling*. Procedia CIRP, 2018. **78**: p. 307-312.
  57. Pavlycheva, N.K., *Diffraction gratings for spectral devices*. Journal of Optical Technology, 2022. **89**(3): p. 142-150.
  58. Salo, D., D.M. Kim, and M.Y. Berezin, *Wavelength-dependent measurement of contrast in NIR and extended NIR spectral range (650-1600 nm) in phantoms*. in *Optical Biopsy XII*. 2014. SPIE.
  59. Fowler, J.E. *Compressive pushbroom and whiskbroom sensing for hyperspectral remote-sensing imaging*. in *2014 IEEE international conference on image processing (ICIP)*. 2014. IEEE.
  60. Striova, J., A. Dal Fovo, and R. Fontana, *Reflectance imaging spectroscopy in heritage science*. La Rivista del Nuovo Cimento, 2020. **43**: p. 515-566.
  61. ANITHA, D. and S.C.V.M. VIDYALAYA, *COURSE MATERIAL REMOTE SENSING & GIS*.
  62. Qian, S.-E., *Hyperspectral satellites, evolution, and development history*. IEEE Journal of Selected Topics in Applied Earth Observations and Remote Sensing, 2021. **14**: p. 7032-7056.
  63. Reuter, D.C., et al., *The Thermal Infrared Sensor (TIRS) on Landsat 8: Design overview and pre-launch characterization*. Remote Sensing, 2015. **7**(1): p. 1135-1153.
  64. Kampe, T.U., et al. *Airborne remote sensing instrumentation for NEON: Status and development*. in *2011 Aerospace conference*. 2011. IEEE.
  65. Funatomi, T., et al., *Eliminating temporal illumination variations in whisk-broom hyperspectral imaging*. International Journal of Computer Vision, 2022. **130**(5): p. 1310-1324.
  66. Hu, Z., et al., *Wide-swath and high-resolution whisk-broom imaging and on-orbit performance of SDGSAT-1 thermal infrared spectrometer*. Remote Sensing of Environment, 2024. **300**: p. 113887.
  67. Tarde, R.W., M.G. Dittman, and G.E. Kvaran, *Next-generation pushbroom filter radiometers for remote sensing*. in *Earth Observing Systems XVII*. 2012. SPIE.
  68. Cross, R.E., *Optical Spectroscopy Instrumentation for the Characterisation of Wide Band Gap Materials*. 2015, Aberystwyth University.
  69. Coulter, D., P. Hauff, and W. Kerby, *Airborne hyperspectral remote sensing*. in *Proceedings of Exploration*. 2007.
  70. Gupta, R. and R.I. Hartley, *Linear pushbroom cameras*. IEEE Transactions on pattern analysis and machine intelligence, 1997. **19**(9): p. 963-975.
  71. Dorja, C., *Pushbroom sensor modelling for HYPPOS telescope calibration*.
  72. Johnson, B.R., T.U. Kampe, and M. Kuester, *Development of airborne remote sensing instrumentations for NEON*. in

- Remote Sensing and Modeling of Ecosystems for Sustainability VII*. 2010. SPIE.
73. Gartley, M. and J. Schott, *Serendipitous imaging of space objects with the advanced land imager*. IEEE Journal of Selected Topics in Applied Earth Observations and Remote Sensing, 2012. **6**(2): p. 440-445.
  74. Johnson, T.P., *Optical System Design and Distortion Control of Wide Field of View, All-Reflective Imagers*. 2019, The University of Arizona.
  75. Erdogan, T., *Optical filters for wavelength selection in fluorescence instrumentation*. Current protocols in cytometry, 2011. **56**(1): p. 2.4. 1-2.4. 25.
  76. Li, Q., et al., *Review of spectral imaging technology in biomedical engineering: achievements and challenges*. Journal of biomedical optics, 2013. **18**(10): p. 100901-100901.
  77. Peng, J., et al., *Analysis of image motion for optical remote sensing satellites staring imaging with area-array detectors*. Applied Optics, 2023. **62**(10): p. 2470-2478.
  78. Magnan, P., *Single-photon imaging for astronomy and aerospace applications*. Single-Photon Imaging, 2011: p. 301-327.
  79. Bhan, R. and V. Dhar, *Recent infrared detector technologies, applications, trends and development of HgCdTe based cooled infrared focal plane arrays and their characterization*. Opto-Electronics Review, 2019. **27**(2): p. 174-193.
  80. Gupta, N. *Development of staring hyperspectral imagers*. in *2011 IEEE Applied Imagery Pattern Recognition Workshop (AIPR)*. 2011. IEEE.
  81. Ortega, S., et al., *Hyperspectral push-broom microscope development and characterization*. IEEE Access, 2019. **7**: p. 122473-122491.
  82. Vollmerhausen, R., R. Driggers, and N. Vision. *Modeling the target acquisition performance of staring array imagers*. in *Proc. IRIS Passive Sensors*. 1998.
  83. Murphy, J.G., *Staring focal plane array system modeling*. 1989, Citeseer.
  84. Li, P., Y. Dong, and H. Li, *Staring Imaging Real-Time Optimal Control Based on Neural Network*. International Journal of Aerospace Engineering, 2020. **2020**(1): p. 8822223.
  85. Yang, G., et al., *The DOM generation and precise radiometric calibration of a UAV-mounted miniature snapshot hyperspectral imager*. Remote Sensing, 2017. **9**(7): p. 642.
  86. Yuan, X., D.J. Brady, and A.K. Katsaggelos, *Snapshot compressive imaging: Theory, algorithms, and applications*. IEEE Signal Processing Magazine, 2021. **38**(2): p. 65-88.
  87. Hagen, N., et al., *Snapshot advantage: a review of the light collection improvement for parallel high-dimensional measurement systems*. Optical Engineering, 2012. **51**(11): p. 111702-111702.
  88. Wagadarikar, A.A., et al. *Spectral image estimation for coded aperture snapshot spectral imagers*. in *Image Reconstruction from Incomplete Data V*. 2008. Spie.
  89. Gano, B., et al., *Drone-based imaging sensors, techniques, and applications in plant phenotyping for crop breeding: A comprehensive review*. The Plant Phenome Journal, 2024. **7**(1): p. e20100.
  90. Ding, K., et al., *Snapshot spectral imaging: from spatial-spectral mapping to metasurface-based imaging*. Nanophotonics, 2024. **13**(8): p. 1303-1330.
  91. Uto, K., et al., *Development of a low-cost hyperspectral whiskbroom imager using an optical fiber bundle, a swing mirror, and compact spectrometers*. IEEE Journal of Selected Topics in Applied Earth Observations and Remote Sensing, 2016. **9**(9): p. 3909-3925.
  92. Soffer, R.J., et al., *Validation of airborne hyperspectral imagery from laboratory panel characterization to image quality assessment: implications for an arctic peatland surrogate simulation site*. Canadian Journal of Remote Sensing, 2019. **45**(3-4): p. 476-508.
  93. Xing, C., et al., *VOCs hyperspectral imaging: A new insight into evaluate emissions and the corresponding health risk from industries*. Journal of Hazardous Materials, 2024. **461**: p. 132573.
  94. Addabbo, P., et al., *The hyperspectral unmixing of trace-gases from ESA SCIAMACHY reflectance data*. IEEE Geoscience and Remote Sensing Letters, 2015. **12**(10): p. 2130-2134.
  95. Huang, C.-H., et al., *An Edge and Trustworthy AI UAV System With Self-Adaptivity and Hyperspectral Imaging for Air Quality Monitoring*. IEEE Internet of Things Journal, 2024.
  96. Ahmadian Marj, A., M.R. Mobasheri, and A.A. Matkan, *Quantitative assessment of different air pollutants (QADAP) using daily MODIS images*. International Journal of Environmental Research, 2017. **11**: p. 523-534.
  97. Just, A.C., et al., *Using high-resolution satellite aerosol optical depth to estimate daily PM<sub>2.5</sub> geographical distribution in Mexico City*. Environmental science & technology, 2015. **49**(14): p. 8576-8584.
  98. Su, X., et al., *Intelligent and scalable air quality monitoring with 5G edge*. IEEE Internet Computing, 2021. **25**(2): p. 35-44.
  99. Kalajdjieski, J., et al., *Air pollution prediction with multi-modal data and deep neural networks*. Remote Sensing, 2020. **12**(24): p. 4142.
  100. Bakirci, M., *Evaluating the impact of unmanned aerial vehicles (UAVs) on air quality management in smart cities: A comprehensive analysis of transportation-related pollution*. Computers and Electrical Engineering, 2024. **119**: p. 109556.
  101. Janarthanan, R., et al., *A deep learning approach for prediction of air quality index in a metropolitan city*. Sustainable Cities and Society, 2021. **67**: p. 102720.
  102. Amato, F., et al., *A novel framework for spatio-temporal prediction of environmental data using deep learning*. Scientific reports, 2020. **10**(1): p. 22243.
  103. Din, A.U., et al., *How sustainable transportation can utilize climate change technologies to mitigate climate change*. Sustainability, 2023. **15**(12): p. 9710.
  104. Jiang, Q., et al., *Feasibility of using visible and near-infrared reflectance spectroscopy to monitor heavy metal contaminants in urban lake sediment*. Catena, 2018. **162**: p. 72-79.
  105. Cai, X., et al., *Remote sensing identification of urban water pollution source types using hyperspectral data*. Journal of Hazardous Materials, 2023. **459**: p. 132080.
  106. Pan, X., et al., *Evaluation of eutrophication in jiaozhou bay via water color parameters determination with UAV-borne hyperspectral imagery*. Atmosphere, 2023. **14**(2): p. 387.
  107. Leung, J.-H., et al., *Water pollution classification and detection by hyperspectral imaging*. Optics Express, 2024. **32**(14): p. 23956-23965.
  108. Fu, X., et al., *Underwater hyperspectral target detection with band selection*. Remote Sensing, 2020. **12**(7): p. 1056.
  109. Rianza, A., et al., *Monitoring acidic water in a polluted river with hyperspectral remote sensing (HyMap)*. Hydrological Sciences Journal, 2015. **60**(6): p. 1064-1077.
  110. Li, Q., et al., *A Joint Framework for Underwater Hyperspectral Image Restoration and Target Detection With Conditional Diffusion Model*. IEEE Journal of Selected Topics in Applied Earth Observations and Remote Sensing, 2024.
  111. Hough, I.M., P.H. Warren, and J.D. Shucksmith, *Designing an environmental flow framework for impounded river systems through modelling of invertebrate habitat quality*. Ecological Indicators, 2019. **106**: p. 105445.
  112. Qi, J., et al., *A self-improving framework for joint depth estimation and underwater target detection from*

- hyperspectral imagery*. Remote Sensing, 2021. **13**(9): p. 1721.
113. Yuan, A., et al., *A low-cost edge AI-chip-based system for real-time algae species classification and HAB prediction*. Water Research, 2023. **233**: p. 119727.
114. Yu, Z., et al., *Aquatic plants detection in crab ponds using UAV hyperspectral imagery combined with transformer-based semantic segmentation model*. Computers and Electronics in Agriculture, 2024. **227**: p. 109656.
115. Furlanetto, R.H., et al., *Hyperspectral Data for Early Identification and Classification of Potassium Deficiency in Soybean Plants (Glycine max (L.) Merrill)*. Remote Sensing, 2024. **16**(11): p. 1900.
116. Banerjee, B.P., S. Raval, and P. Cullen, *UAV-hyperspectral imaging of spectrally complex environments*. International Journal of Remote Sensing, 2020. **41**(11): p. 4136-4159.
117. Ferral, A., et al., *Bringing satellite and nanotechnologies together: unifying strengths against pollution and climate change*. Frontiers in Nanotechnology, 2024. **6**: p. 1332820.
118. Dimobe, K., et al., *Identification of driving factors of land degradation and deforestation in the Wildlife Reserve of Bontioli (Burkina Faso, West Africa)*. Global Ecology and Conservation, 2015. **4**: p. 559-571.
119. Mao, D., et al., *Diverse policies leading to contrasting impacts on land cover and ecosystem services in Northeast China*. Journal of Cleaner Production, 2019. **240**: p. 117961.
120. Feng, S., et al., *Land use/land cover mapping based on GEE for the monitoring of changes in ecosystem types in the upper Yellow River basin over the Tibetan Plateau*. Remote Sensing, 2022. **14**(21): p. 5361.
121. Thangavel, K., et al., *Autonomous satellite wildfire detection using hyperspectral imagery and neural networks: A case study on australian wildfire*. Remote Sensing, 2023. **15**(3): p. 720.
122. Chaity, M.D. and J. van Aardt, *Exploring the Limits of Species Identification via a Convolutional Neural Network in a Complex Forest Scene through Simulated Imaging Spectroscopy*. Remote Sensing, 2024. **16**(3): p. 498.
123. Brook, A., et al., *A smart multiple spatial and temporal resolution system to support precision agriculture from satellite images: Proof of concept on Aglianico vineyard*. Remote Sensing of Environment, 2020. **240**: p. 111679.
124. Mäyryä, J., et al., *Tree species classification from airborne hyperspectral and LiDAR data using 3D convolutional neural networks*. Remote Sensing of Environment, 2021. **256**: p. 112322.
125. Stuart, M.B., et al., *Low-cost hyperspectral imaging system: Design and testing for laboratory-based environmental applications*. Sensors, 2020. **20**(11): p. 3293.
126. Stuart, M.B., et al., *High-resolution hyperspectral imaging using low-cost components: Application within environmental monitoring scenarios*. Sensors, 2022. **22**(12): p. 4652.
127. Yi, L., et al., *Seamless mosaicking of uav-based push-broom hyperspectral images for environment monitoring*. Remote Sensing, 2021. **13**(22): p. 4720.
128. Horstrand, P., et al., *A UAV platform based on a hyperspectral sensor for image capturing and on-board processing*. IEEE Access, 2019. **7**: p. 66919-66938.
129. Radulescu, M., et al., *Optimizing mineral identification for sustainable resource extraction through hybrid deep learning enabled FinTech model*. Resources Policy, 2024. **89**: p. 104692.
130. Nie, P., et al., *Classification of hybrid seeds using near-infrared hyperspectral imaging technology combined with deep learning*. Sensors and Actuators B: Chemical, 2019. **296**: p. 126630.
131. Ahmed, M.T., A. Villordon, and M. Kamruzzaman, *Comparative analysis of hyperspectral Image reconstruction using deep learning for agricultural and biological applications*. Results in Engineering, 2024. **23**: p. 102623.
132. Li, K.-Y., et al., *Toward automated machine learning-based hyperspectral image analysis in crop yield and biomass estimation*. Remote Sensing, 2022. **14**(5): p. 1114.
133. Wajs, J., et al., *Modern solution for fast and accurate inventorization of open-pit mines by the active remote sensing technique—case study of mikoszków granite mine (lower silesia, SW Poland)*. Energies, 2021. **14**(20): p. 6853.
134. Yang, G., et al., *Enhanced mangrove vegetation index based on hyperspectral images for mapping mangrove*. ISPRS Journal of Photogrammetry and Remote Sensing, 2022. **189**: p. 236-254.
135. Zhao, G., et al., *Joint classification of hyperspectral and LiDAR data using a hierarchical CNN and transformer*. IEEE Transactions on Geoscience and Remote Sensing, 2022. **61**: p. 1-16.
136. Zhang, M., et al., *Hyperspectral and LiDAR data classification based on structural optimization transmission*. IEEE Transactions on Cybernetics, 2022. **53**(5): p. 3153-3164.
137. Guo, Z., et al., *Ultimate spatial resolution realisation in optical frequency domain reflectometry with equal frequency resampling*. Sensors, 2021. **21**(14): p. 4632.
138. McIsaac, M.A., et al., *The impact of image resolution on power, bias, and confounding: a simulation study of ambient light at night exposure*. Environmental epidemiology, 2021. **5**(2): p. e145.
139. Carle, M.V., L. Wang, and C.E. Sasser, *Mapping freshwater marsh species distributions using WorldView-2 high-resolution multispectral satellite imagery*. International journal of remote sensing, 2014. **35**(13): p. 4698-4716.
140. Helmer, E.H. and B. Rufenacht, *Cloud-free satellite image mosaics with regression trees and histogram matching*. Photogrammetric Engineering & Remote Sensing, 2005. **71**(9): p. 1079-1089.
141. Bu, L., et al., *Hyperspectral super-resolution reconstruction network based on hybrid convolution and spectral symmetry preservation*. Remote Sensing, 2023. **15**(13): p. 3225.
142. Reale, R., et al., *A low-cost, label-free microfluidic scanning flow cytometer for high-accuracy quantification of size and refractive index of particles*. Lab on a Chip, 2023. **23**(8): p. 2039-2047.
143. Zheng, P., et al., *A parallel unmixing-based content retrieval system for distributed hyperspectral imagery repository on cloud computing platforms*. Remote Sensing, 2021. **13**(2): p. 176.
144. Yi, W., et al., *Comparative Analysis of Manifold Learning-Based Dimension Reduction Methods: A Mathematical Perspective*. Mathematics, 2024. **12**(15): p. 2388.
145. Morales, G., et al., *Hyperspectral dimensionality reduction based on inter-band redundancy analysis and greedy spectral selection*. Remote Sensing, 2021. **13**(18): p. 3649.
146. Ambler, G., R.Z. Omar, and P. Royston, *A comparison of imputation techniques for handling missing predictor values in a risk model with a binary outcome*. Statistical methods in medical research, 2007. **16**(3): p. 277-298.
147. Lighthart, A., C. Catal, and B. Tekinerdogan, *Analyzing the effectiveness of semi-supervised learning approaches for opinion spam classification*. Applied Soft Computing, 2021. **101**: p. 107023.
148. Ahmad, M., et al., *Multiclass non-randomized spectral-spatial active learning for hyperspectral image classification*. Applied Sciences, 2020. **10**(14): p. 4739.
149. da Silva, L.A., et al., *Spatio-temporal deep learning-based methods for defect detection: An industrial application study case*. Applied Sciences, 2021. **11**(22): p. 10861.
150. Kizel, F. and J.A. Benediktsson, *Spatially enhanced spectral unmixing through data fusion of spectral and visible images from different sensors*. Remote Sensing, 2020. **12**(8): p. 1255.

151. Wu, T., et al., *Channel Activity Remote Sensing Retrieval Model: A Case Study of the Lower Yellow River*. Remote Sensing, 2023. **15**(14): p. 3636.
152. Jia, G., et al., *Detection and correction of spectral shift effects for the airborne prism experiment*. IEEE Transactions on Geoscience and Remote Sensing, 2017. **55**(11): p. 6666-6679.
153. Baumgart, J., D. Mikołajewski, and J.M. Czerniak, *Taking Flight for a Greener Planet: How Swarming Could Help Monitor Air Pollution Sources*. Electronics, 2024. **13**(3): p. 577.
154. Song, H., et al., *Underwater spectral imaging system based on liquid crystal tunable filter*. Journal of Marine Science and Engineering, 2021. **9**(11): p. 1206.
155. Zhou, J., et al., *Detection of volatile organic compounds using mid-infrared silicon nitride waveguide sensors*. Scientific Reports, 2022. **12**(1): p. 5572.
156. Xiao, Y., et al., *Simulating return signals of a spaceborne high-spectral resolution lidar channel at 532 nm*. Optics Communications, 2018. **417**: p. 89-96.
157. Zhang, L., et al., *A hyperspectral band selection method based on sparse band attention network for maize seed variety identification*. Expert Systems with Applications, 2024. **238**: p. 122273.
158. Fan, S., et al., *Data fusion of two hyperspectral imaging systems with complementary spectral sensing ranges for blueberry bruising detection*. Sensors, 2018. **18**(12): p. 4463.
159. Zatta, D., et al., *Comparative Analysis of VOC Purification Techniques in Complex Cooking Emissions: Adsorption, Photocatalysis and Combined Systems*. 2023.
160. Xu, J., et al. *Towards Real-World Adverse Weather Image Restoration: Enhancing Clearness and Semantics with Vision-Language Models*. in *European Conference on Computer Vision*. 2025. Springer.
161. Laamrani, A., et al., *Ensemble identification of spectral bands related to soil organic carbon levels over an agricultural field in Southern Ontario, Canada*. Remote Sensing, 2019. **11**(11): p. 1298.
162. Song, M., et al., *Multiobjective optimization-based hyperspectral band selection for target detection*. IEEE Transactions on Geoscience and Remote Sensing, 2022. **60**: p. 1-22.
163. Lopriore, L., *Hardware/compiler memory protection in sensor nodes*. International Journal of Communications, Network and System Sciences, 2008. **1**(3): p. 235.
164. Guo, T., et al., *Miniaturized Hyperspectral Imager Utilizing a Reconfigurable Filter Array for Both High Spatial and Spectral Resolutions*. Nano Letters, 2024. **24**(36): p. 11156-11162.
165. Thuillier, G., et al., *Observation of the UV solar spectral irradiance between 200 and 350 nm during the Atlas 1 mission by the SOLSPEC spectrometer*. Solar Physics, 1997. **171**: p. 283-302.
166. Shea, Y.L., et al., *An entropy framework for evaluating reflectance observations for climate studies*. Earth and Space Science, 2022. **9**(7): p. e2019EA000795.